Microchimica Acta
https://doi.org/10.1007/s00604-018-2884-5

ORIGINAL PAPER

Aptamer based voltammetric biosensor for *Mycobacterium tuberculosis* antigen ESAT-6 using a nanohybrid material composed of reduced graphene oxide and a metal-organic framework

Linlin Li[1] · Yonghua Yuan[1] · Yongjie Chen[1] · Pu Zhang[1] · Yan Bai[1] · Lijuan Bai[1]

Received: 26 March 2018 / Accepted: 25 June 2018

Abstract

The 6-kDa early secretory antigenic target referred to as ESAT-6 is a virulence factor secreted by *Mycobacterium tuberculosis* (MTB). This work describes a voltammetric aptasensor for ultrasensitive detection of ESAT-6. Reduced graphene oxide doped with metal-organic framework (MOF-rGO) was deposited on a glassy carbon electrode (GCE). This increases the immobilization of electroactive Toluidine Blue (TB) and facilitates the electron transfer from TB to the modified GCE. Platinum/gold core/shell (Pt@Au) nanoparticles were used to assemble thiolated ESAT-6 binding aptamer (EBA) on a modified electrode and to further amplify the response to TB. The modified GCE, typically operated at −0.36 V (vs. SCE), has a linear response in 1.0×10^{-4} to 2.0×10^{2} ng·mL^{-1} ESAT-6 concentration range, and the limit of detection (LOD) for ESAT-6 is as low as 3.3×10^{-5} ng·mL^{-1}. It exhibits satisfactory specificity and reproducibility when analyzing spiked human serum.

Keywords Aptasensor · Pt@Au nanoparticles · Cyclic voltammetry · Electrochemical impedance spectroscopy · Signal amplification · Electrochemical detection · Effective surface area

Introduction

Tuberculosis is one of the most prevalent and fatal infectious diseases caused by *Mycobacterium tuberculosis* (MTB), which seriously threatens people's life safety. Because of its long course of treatment, low cure rate and high recurrence rate, it causes a great burden on the national economy [1]. Thus, rapid and accurate detection of MTB has important significance for the early diagnosis and control of tuberculosis. This can reduce the aggravation of patient's condition due to misdiagnosis [2]. At present, the conventional methods for MTB diagnosis exist several defects, which limit theirs wide application. For example, bacterial culture takes a long time and its positive rate is low [3, 4], polymerase chain reaction (PCR) has high technical requirements and low reproducibility [5, 6], and the enzyme-linked immunosorbent assay (ELISA) often suffers from low specificity [7, 8]. Therefore, in order to find more ideal MTB diagnostic assays for clinical use, novel detection approaches and biomarkers are being explored. Biosensors targeting MTB related components have been demonstrated to be a promising MTB detection technique.

The current study illustrates that the qualitative and quantitative analyses of MTB antigen components and their own protective cytokines (MPT64, 10-kDa culture filtrate protein (CFP-10) and 6-kDa early secreted antigenic target (ESAT-6), etc.) have clinical significance in the diagnosis, treatment and control of tuberculosis [9, 10]. Compared to other antigens, ESAT-6, a low molecular weight secreted protein isolated from short-term MTB culture filtrates, shows a higher specificity [11, 12]. It is encoded by the Rv3874 gene in the RD1 region. Genomics analysis revealed that RD1 was present in pathogenic MTB genomes, whereas this region was absent in all BCG vaccine strains [13]. Detection of ESAT-6 can avoid the false positive results caused by BCG vaccination. Moreover, ESAT-6 appears early when the organism is infected by MTB and plays an important role in the early diagnosis

Linlin Li and Yonghua Yuan contributed equally to this work.

Electronic supplementary material The online version of this article (https://doi.org/10.1007/s00604-018-2884-5) contains supplementary material, which is available to authorized users.

✉ Lijuan Bai
bailijua88@126.com

[1] Engineering Technology Research Center for Pharmacodynamic Evaluation of Chongqing, College of Pharmacy, Chongqing Medical University, Chongqing 400016, People's Republic of China

Published online: 17 July 2018

of tuberculosis. Therefore, ESAT-6 can be used as a desirable candidate for detection of MTB [14, 15]. With the in-depth study of nucleic acids, aptamers, artificial synthetic single-stranded oligonucleotides, are widely employed as identification elements in the field of basic research, biological detection and targeted drug delivery [16, 17]. Compared with traditional detection approaches, aptamer-based biosensors (aptasensors) possess the advantages of high sensitivity and selectivity, fast response and low cost, has broad application prospects in disease diagnosis, environmental monitoring and bioanalysis [18, 19]. To date, aptasensor for ESAT-6 detection has rarely been reported. In order to obtain higher sensitivity of electrochemical aptasensor for trace analysis, variety of signal amplification strategies have been extensively studied, particularly in the application of nanomaterials [20, 21]. Metal-organic framework (MOF) has attracted great attention in supercapacitors [22] and biosensors due to its porous structure and high theoretical capacity [23, 24]. For example, Tang and co-workers developed a sandwich-type immunosensor for the detection of galectin-3 based on Fe-MOF nanomaterial with a low detection limit [25]. However, the application of MOF in electrochemical sensor often suffers from its poor electronic conductivity. Fortunately, reduced graphene oxide (rGO) is a fascinating nanomaterial whose high conductivity has overcome this hurdle [26]. Accordingly, MOF doped rGO (MOF-rGO) nanohybrid may possess many favorable properties, including larger specific surface area, higher conductivity and stability, which not only increases the immobilization of electroactive material, but also facilitates the electron transfer from signal substance to the electrode [27]. Furthermore, a nanocomposite functionalized with poly (diallyldimethylammonium chloride) (P-MOF-rGO) prevents the agglomeration of MOF-rGO and enhances the dispersity and stability of the nanocomposite.

In this study, a label-free electrochemical aptasensor with a P-MOF-rGO nanohybrid as the sensitive sensing platform was fabricated for ultrasensitive detection of ESAT-6, which overcame the challenges of the traditional MTB detection methods such as unsatisfactory LOD and specificity, complicated operation and long time-consuming. Firstly, P-MOF-rGO nanocomposite was employed to enhance the loading of electroactive toluidine blue (TB). Then, Platinum aurum core shell (Pt@Au) nanoparticles [28, 29] that hold more excellent electrical properties than single metal nanoparticles provided abundant active sites for the immobilization of thiolated ESAT-6 binding aptamer (EBA) and further amplified the electrochemical response signal of TB. After the specific recognition between ESAT-6 antigen and EBA, significant change of electrochemical signal indicated that the aptasensor was successfully constructed. Compared with other sensors used for MTB detection [30, 31], this aptasensor is more specific in the choice of this target. In addition, the nanocomposite employed to modify the electrode possesses a larger electroactive specific surface area, which is conducive to increase the immobilization of the electroactive substances.

Materials and methods

Reagents and materials

ESAT-6 was obtained from Prospec-Tany Technology Co., Ltd. (Israel). TB, PDDA, 2-aminoterephthalic acid, $K_3[Fe(CN)_6]$ and $K_4[Fe(CN)_6]$ were purchased from Sigma-Aldrich Chemical Co. (USA, www.sigmaaldrich.com). Graphene oxide (GO) was furnished by XFNANO Nanotechnology Co., Ltd. (Nanjing, China, www.xfnano.com). N, N-dimethylformamide (DMF) and ethanol were obtained from Kelong (Chengdu, China, www.cdkelong.com). $FeCl_3 \cdot 6H_2O$ was achieved from Chongqing Chuandong Chemical Group Co., Ltd. (Chongqing, China, www.cqchemgroup.com). Bovine serum albumin (BSA), ascorbic acid (AA), chloroauric acid ($HAuCl_4$) and chloroplatinic acid (H_2PtCl_6) were obtained from J&K Scientific Co., Ltd. (Beijing, China, www.Jkchemical.com). CFP-10 was provided by Biomart Biotechnology Co., Ltd. (Beijing, China). Healthy human serums used for the recovery experiment were obtained from the First Affiliated Hospital of Chongqing Medical University (Chongqing, China). The EBA was purchased from Sangon Biological Engineering Technology Ltd. (Shanghai, China, www.sangon.com), and the sequence of sythesized oligonucleotide as follow [32, 33]:

EBA: 5′-SH-$(CH_2)_6$-GGG AGC TCA GAA TAA ACG CTC AAC CTC CCT GGG TCA CCA TAG ACT CCA TCT AAG ATG CTT CGA CAT GAG GCC CGG ATC-3′

20 mM TES buffer (pH 7.4) containing 1 mM EDTA, 0.1 mM NaCl and 10 mM Tris (2-carboxyethy) phosphine hydrochloride was used to prepare the oligonucleotide solution. $Fe(CN)_6^{3-/4-}$ solution (5 mM) containing 0.1 M KCl was employed to calculate the effective surface area of different modified electrodes and monitor the each step of the aptasensor construction process. The electrolyte solution used for electrochemical characterization was phosphate buffer (0.1 M, pH 7.0) containing 10 mM KCl and 2 mM $MgCl_2$. All other reagents used in the experiment were analytical reagent grade and without additional treatment. Ultrapure water (with the resistivity of 18.2 MΩ.cm) from a Millipore Mill-Q purification system was used throughout the course of the experiment.

Apparatus and measurements

All electrochemical experiments were carried out with a CHI660E electrochemical workstation (Shanghai Chenhua Instrument, China) at room temperature using in a conventional three-electrodes system: a platinum wire auxiliary

electrode, a saturated calomel reference electrode (SCE) and the modified glassy carbon electrode (GCE, Φ = 4 mm) as working electrode. Cyclic voltammetry (CV) scan, taken from −0.70 to 0.30 V (vs. SCE) at a scan rate of 100 mV/s in phosphate buffer (pH 7.0), was employed to analyse the performance of the aptasensor. Electrochemical impedance spectroscopy (EIS) was used to investigate fabrication process was taken from −0.20 to 0.60 V (vs. SCE) at a scan rate of 100 mV/s in 5.0 mM $Fe(CN)_6^{3-/4-}$ solution. The size and morphology characterization of nanomaterials was supplied by transmission electron microscopy (TEM) (H600, Hitachi Instrument, Japan) and field emission scanning electron microscopy (FESEM, JSM7800F, Japan). Fourier-transform infrared (FTIR) spectroscopy (Thermo Nicole, USA) and X-ray photoelectron spectroscopy (XPS) (Thermo, ESCALAB 250, USA) were used to characterize the structure and elemental composition of nanomaterials .

Preparation of MOF and P-MOF-rGO

MOF were prepared according to the literature [34] with slight modification. Detailed description of the preparation process was given in ST1 (see Electronic Supplementary Material).

The synthesis method of P-MOF-rGO (1.0 mg/mL) was as follows: 5 mg GO was added into 5 mL ultrapure water and vigorously sonicated for 3 min. Subsequently, 40 μL of PDDA (20%) was added to the above solution under stirring for 30 min at room temperature. Then 100 μL hydrazine hydrate (80%) was added to the solution and the mixture was placed in a water bath at 90 °C for 4 h. After that, 5 mL MOF (2.0 mg/mL) was added into the dispersion and stirred for 24 h. The product was centrifuged and washed with ultrapure water to remove surplus reactants. The precipitate was then redispersed homogeneously in 10 mL of ultrapure water and stored at 4 °C before use.

Preparation of Pt@Au nanoparticles

First of all, 20 mL colloidal Au nanoparticles were prepared (see Electronic Supplementary Material) and added into 30 mL ultrapure water and heating to 80 °C. Then 2.5 mL H_2PtCl_6 was quickly added into the mixture with vigorous stirring. After that, 1.75 mL (1%) AA was added into the solution mentioned above and was heated to reflux until the color of black did not change. The obtained Pt@Au nanoparticles was transferred to 50 mL brown volumetric flask and stored at 4 °C.

Fabrication of the aptasensor

Prior to constructing the aptasensor, the surface of electrode was polished carefully with 0.3 μm and 0.05 μm alumina slurry in this order. It was ultrasonically washed several times with ultrapure water until the solution was no longer cloudy, and then washed successively with ethanol and ultrapure water for 5 min each.

Afterwards, a droplet of 10 μL P-MOF-rGO solution was cast onto the pretreated electrode and dried in air. Then 5 μL TB solution was added to the surface of the modified electrode overnight and rinsed with ultrapure water, followed by adding 8 μL Pt@Au nanoparticles for 1 h. Then 20 μL EBA (2 μM) was dropped onto the electrode surface for 8 h and blocked with 10 μL BSA (3%) for 1 h. After washing with ultrapure water, the prepared electrode was incubated with 20 μL of ESAT-6 solution with different concentrations at room temperature for 1 h. The electrochemical response signal originated from TB changed before and after the specific recognition between EBA and target ESAT-6, which gave the quantitative criteria for electrochemical detection of ESAT-6 antigen. The stepwise fabrication process of the aptasensor was depicted in Scheme 1.

Results and discussion

Choice of materials

MOF has been chosen as electrode material due to its uniquely porous structure, this structure endowes it with large specific surface area and the ability to promote electron transfer. However, poor conductivity limits its application in sensor field. To overcome this obstacle, we have chosen rGO doping into MOF. rGO possesses features of high electrical conductivity, excellent thermal stability, outstanding flexibility and susceptibility to electrochemical modifications, the incorporation of the carbon layer greatly improves the electrical conductivity of the MOF.

Biosensors serving MOF-rGO hybrid nanocomposite as matrix have been reported, which exhibited high sensitivity and reliability in the simultaneous quantitative electrochemical determination of catechol and hydroquinone [35].

In order to further promote the electrochemical performance of the designed aptasensor, we have functionalized the MOF-rGO hybrid nanocomposite with PDDA. As a strong cationic polyelectrolyte and high-molecular antistatic agent, the incorporation of PDDA prevents the agglomeration of MOF-rGO and enhances the dispersity and stability of the nanocomposite. Compared with single nanomaterial, the P-MOF-rGO composite possessed many favorable characteristics, including increased specific surface area (Fig. S4, see Electronic Supplementary Material), improved conductivity and satisfactory film formation. Thus, P-MOF-rGO nanocomposite was chosen as immobilization matrix of aptasensor in our work.

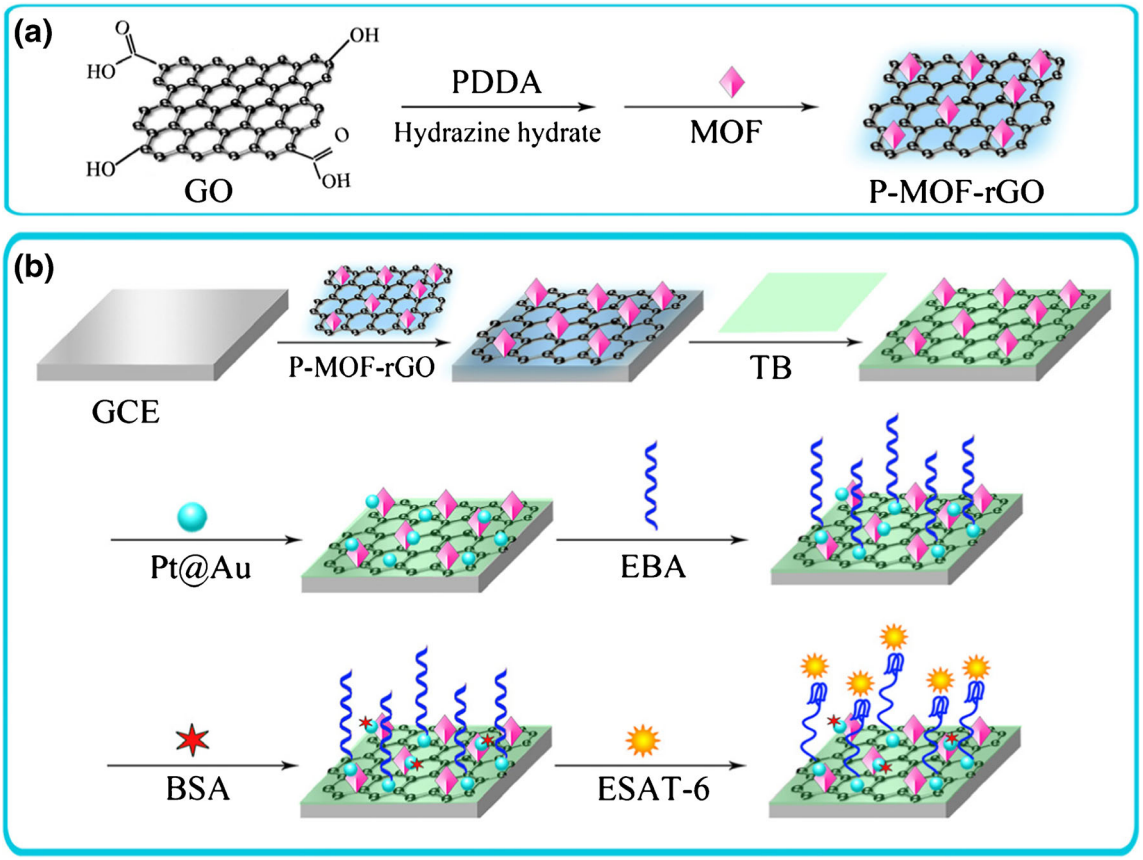

Scheme 1 Schematic illustration of the stepwise construction procedure of the electrochemical aptasensor

Characterization research

Characterization of different nanomaterials

The size and morphology characterization images of the synthesized nanomaterials were supplied by TEM and FESEM. As shown in Fig. 1a, MOF demonstrated regular octahedron structure with a diameter of about 100 nm, while rGO showed a lamella structure with folds (Fig. 1b). As shown in Fig. 1c, a great deal of MOF nanoparticles covered on the surface of rGO homogeneously and densely, indicating the successful preparation of P-MOF-rGO. Pt@Au nanoparticles exhibited a burr-like spherical structure and dispersed uniformly (Fig. 1d).

FTIR and XPS studies

The FTIR spectra studies of P-rGO, MOF and P-MOF-rGO were shown in Fig. S1 (see Electronic Supplementary Material). XPS was further used to confirm the chemical structure and elemental composition of P-MOF-rGO nanohybrid (Fig. S2, see Electronic Supplementary Material).

Electrochemical characterization of the aptasensor

CV was employed to characterize the electrochemical performance of surface-modified electrodes during the fabrication process. As shown in Fig. 2, when the GCE was coated with P-MOF-rGO, the current response (curve b) obviously increased compared with bare GCE (curve a), which ascribed to the fact that increased conductivity due to the synergistic effect of rGO and MOF. After the electroactive TB was modified on the electrode surface, a pair of obvious redox peaks appeared (curve c). When Pt@Au nanoparticles were deposited on the modified GCE, the peak current greatly increased (curve d), attributing to the Pt@Au can significantly enhance the effective surface area and facilitate the electron transfer. It can be seen that the response decreases when the modified electrode was incubated with EBA (curve e), BSA (curve f) and the target (curve g), respectively. The reason was that non-electroactive aptamer and large protein greatly inhibited the electron transfer. In summary, all the experiment results clearly demonstrated the successful construction of the aptasensor.

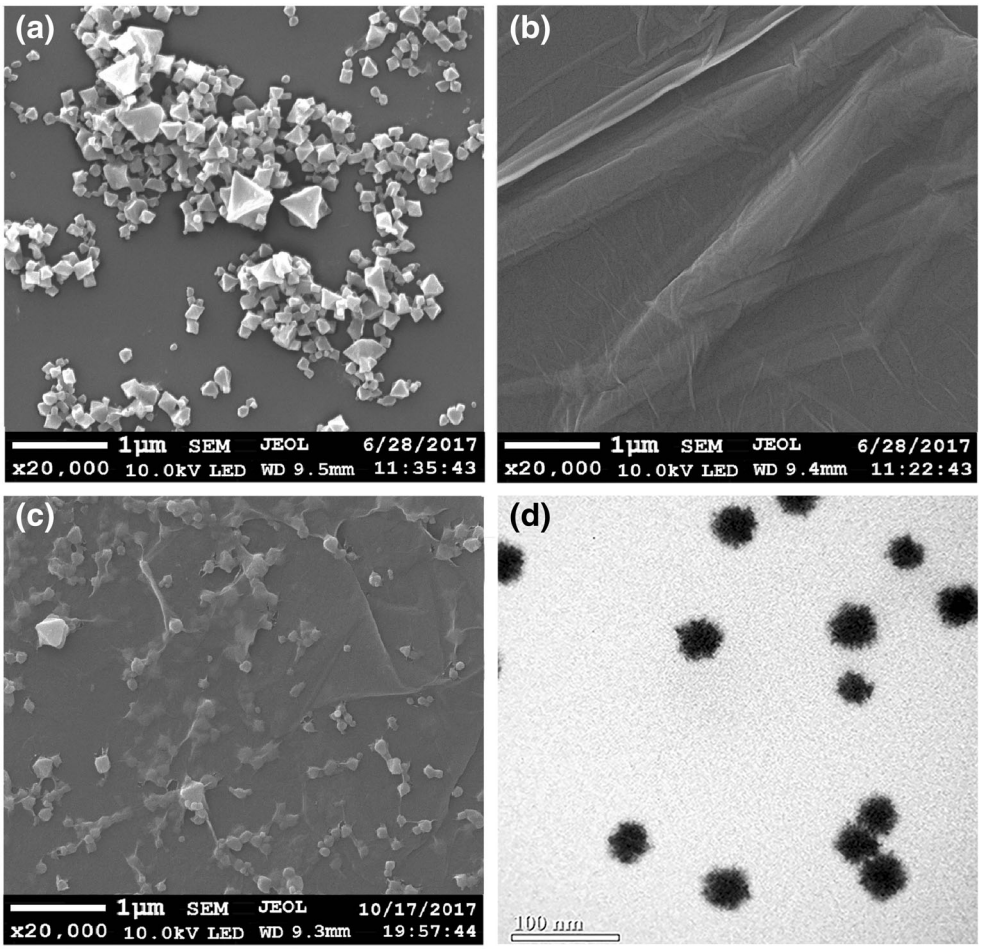

Fig. 1 FESEM images of **a** MOF, **b** rGO nanosheets, **c** P-MOF-rGO nanocomposite and TEM image of **d** Pt@Au nanoparticles

The interfacial properties of the steps of aptasensor construction process were investigated by EIS (Fig. S3, see Electronic Supplementary Material).

The electroactive specific surface area of different modified electrodes was calculated by performing CV measurements at different sweep speeds and the results were shown in Fig. S4 (see Electronic Supplementary Material, ST6).

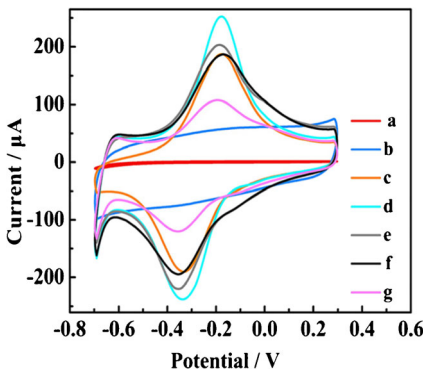

Fig. 2 CV responses for each immobilized step: **a** bare GCE, **b** P-MOF-rGO/GCE, **c** TB/P-MOF-rGO/GCE, **d** Pt@Au/TB/P-MOF-rGO/GCE, **e** EBA/Pt@Au/TB/P-MOF-rGO/GCE, **f** BSA/EBA/Pt@Au/TB/P-MOF-rGO/GCE and **g** ESAT-6/BSA/EBA/Pt@Au/TB/P-MOF-rGO/GCE were taken from −0.70 to 0.30 V (vs. SCE) in phosphate buffer (pH 7.0). The voltage at the peak current was −0.36 V

Optimization of the aptasensor preparation conditions

In order to achieve the optimal analysis performance of the aptasensor, the dosage of TB (1.0 mg/mL) and Pt@Au (0.50 mg/mL) nanoparticles was investigated. As shown in Fig. 3a, with increasing amount of TB incubated on the electrode surface, the peak current increased. It was clearly observed that the current response increased greatly and tended to a constant value at 5 μL. Thus, 5 μL was selected as the optimal volumn of TB. The volume of Pt@Au nanoparticles was explored to provide a favorable platform for immobilizing EBA. As shown in Fig. 3b, as the volume of Pt@Au nanoparticles increased from 3 μL to 8 μL, the current response showed a continuous upward trend, and then the current change tended to be steady when the volume reached to 8 μL. Therefore, 8 μL was chosen as the volume of Pt@Au to modify the electrode .

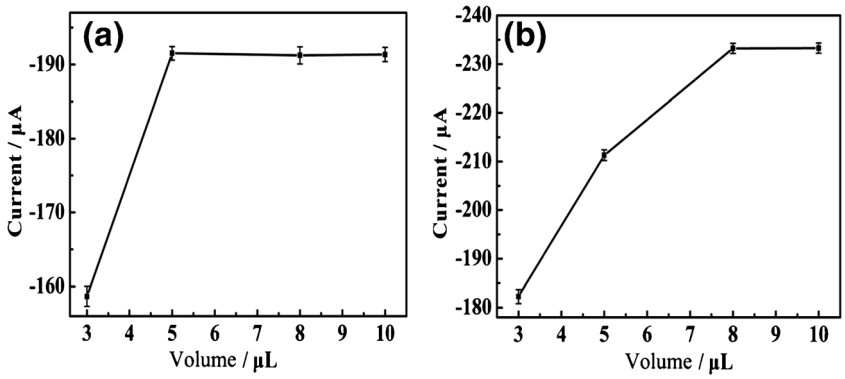

Fig. 3 Signal dependence of the different amounts of (**a**) TB and (**b**) Pt@Au nanoparticles. The error bars represent the standard deviations of three parallel determination results ($n = 3$)

Performance of the aptasensor

Analytical performance of the aptasensor

CV measurement was employed to estimate the quantitative range of the aptasensor by detect ESAT-6 standard solution at various concentrations under the optimal detection conditions in phosphate buffer (pH 7.0). As shown in Fig. 4a, the current responses of the aptasensor gradually reduced with increasing concentrations of target ESAT-6 in the range of 1.0×10^{-5} ng/mL~2.0×10^{3} ng/mL due to the blocking of electron transfer by macromolecules. When the concentration of ESAT-6 is less than 1.0×10^{-4} ng/mL (curve b), there is almost no change in the peak current compared with the bare electrode. This is due to the fact that the concentration of ESAT-6 is so low that it cannot combine with EBA to form enough target-aptamer complexes to cause current changes. When the concentration is higher than 2.0×10^{2} ng/mL, the binding of ESAT-6 to EBA is almost saturated, and the peak current increases slowly. The calibration curve for quantitative determination of ESAT-6 obtained by using the logarithm of the target concentration as the abscissa and the peak current as the ordinate was illustrated in Fig. 4b. A wide linear relationship was observed in the range from 1.0×10^{-4} ng/mL to 2.0×10^{2} ng/mL with a linear regression equation is $I = 10.2$ lg$c$-123. The electrochemical sensitivity was 706 μA ng·mL^{-1} cm^{-2} combined with the effective surface area of electrode. The limit of detection (LOD) of this aptasensor for ESAT-6 was estimated to be 3.3×10^{-5} ng/mL based on the $3\sigma/m$ criterion (where σ is the standard deviation of the blank and m is the slope of the calibration plot). The favorable detection performance was mainly attributed to the synergistic effect of P-MOF-rGO and Pt@Au nanoparticles, which not only promoted the electron transfer, but also provided large electroactive surface for the immobilization of aptamers.

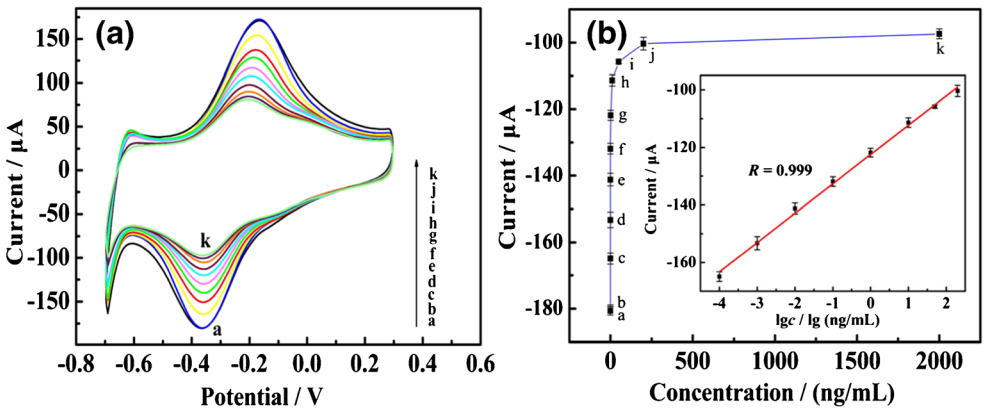

Fig. 4 **a** CV responses of the aptasensor incubated with different concentrations of ESAT-6 standard solution: (*a*) blank, (*b*) 1.0×10^{-5} ng/mL, (*c*) 1.0×10^{-4} ng/mL, (*d*) 1.0×10^{-3} ng/mL, (*e*) 1.0×10^{-2} ng/mL, (*f*) 1.0×10^{-1} ng/mL, (*g*) 1.0 ng/mL, (*h*) 1.0×10^{1} ng/mL, (*i*) 5.0×10^{1} ng/mL, (*j*) 2.0×10^{2} ng/mL, (*k*) 2.0×10^{3} ng/mL in phosphate buffer (pH 7.0) from −0.70 to 0.30 V at a scan rate of 100 mV/s (vs. SCE). **b** Relationship between peak current and ESAT-6 concentrations in the range from 1.0×10^{-5} ng/mL to 2.0×10^{3} ng/mL. Inset showed the calibration plots of CV peak current versus the logarithm of ESAT-6 concentration ($n = 3$). The voltage at the peak current was −0.36 V

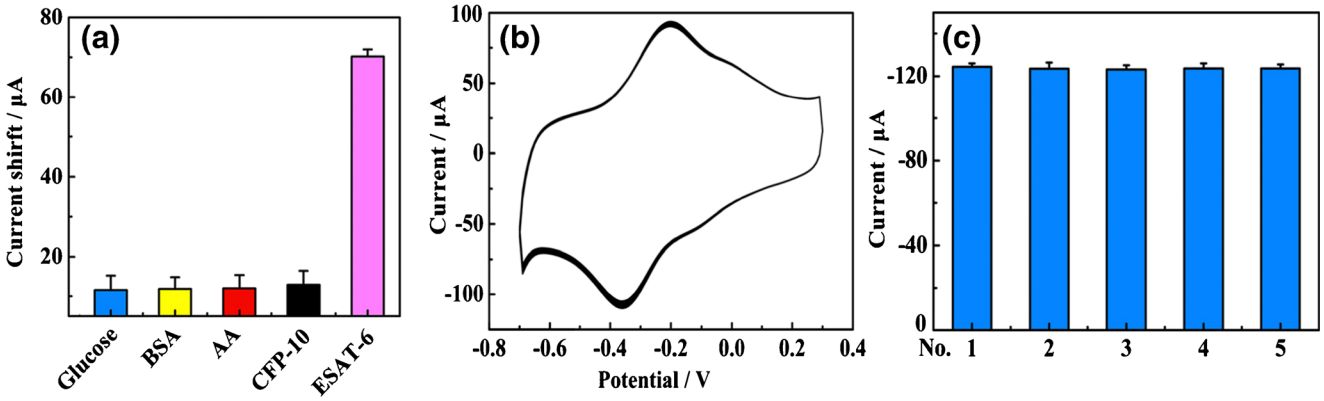

Fig. 5 **a** ESAT-6 (1 ng/mL) against the interference molecules: Glucose (1 ng/mL), BSA (1 ng/mL), AA (1 ng/mL) and CFP-10 (1 ng/mL) ($n = 3$). **b** Stability of the aptasensor incubated with 1 ng/mL ESAT-6 under successive CV scans for 50 cycles. **c** Five different electrodes were scanned CV measurement under the same optimized conditions (n = 3). CV was taken in phosphate buffer (pH 7.0) at a potential ranging from (−0.70 to 0.30) V with a scan rate of 100 mV/s

Specificity, stability and reproducibility of the aptasensor for ESAT-6 detection

Since ESAT-6 was mainly isolated from the MTB culture filtrate, the endogenous molecules coexisting in the serum of tuberculosis patients, such as glucose, BSA, AA and CFP-10, were used to evaluate the specificity of this sensor. Figure 5a showed the corresponding histogram of the aptasensor toward different analytes. Compared with the same concentration of interferents, the specific recognition of target and aptamer caused a significant decrease in the electrochemical signal of the aptasensor, indicating that the sensor had satisfactory selectivity for ESAT-6 detection.

To investigate the stability of the aptasensor, the electrode was taken successive cyclic scans under the optimal conditions. Compared with the initial current response, the response decreased only about 3.5% after 50 cycles' continuous CV scans (Fig. 5b). The consequence demonstrated the electrochemical aptasensor hold a favorable stability.

As shown in Fig. 5c, five electrodes incubated with same concentration of ESAT-6 (1 ng/mL) were analyzed. Under the same optimized conditions, the current responses measured by all electrodes exhibited a similar electrochemical response with a relative standard deviation (RSD) of 2.9%, indicating the aptasensor had acceptable reproducibility.

Moreover, the detection performances of the aptasensor and those of other ESAT-6 test approaches reported in the literatures were compared methodologically, and the results were illustrated in Table S1 (see in Supplementary data, ST7). Accordingly, this aptasensor based on P-MOF-rGO nanocomposite showed a wider linear range with lower detection limit for ESAT-6 detection.

Application for the analysis of serum samples

Because ESAT-6 was mainly isolated from tuberculosis patients' early culture filtrates of MTB, healthy human serum was selected as the matrix for spiked recovery. Recovery experiments used to assess the analytical reliability and application of the aptasensor were performed by standard addition methods. The biosensor was applied to human diluted serum samples spiked with 1.0×10^{-4} ng/mL, 2.0×10^{-1} ng/mL and 2.0×10^{2} ng/mL ESAT-6 solution. As shown in Table S2 (see Electronic Supplementary Material), the recoveries for three concentrations of ESAT-6 was 102%, 99 and 101%, while the RSD was 4.83%, 3.47 and 3.79%, respectively. These results suggested that the aptasensor had the potential application in quantitative detection of ESAT-6 in human serum.

Conclusions

In this work, a specific aptasensor for ultrasensitive detection of ESAT-6 using P-MOF-rGO nanocomposite as immobilization matrix has been successfully developed, it has overcome the challenge of early diagnosis of MTB. The sensor, which used a specific binding of aptamer and ESAT-6 as a recognition element was first reported for the quantitative detection of ESAT-6 antigen. Owing to the synergistic effect of MOF and rGO, a large specific surface (17.0 mm^2) of P-MOF-rGO was provided for the immobilization of electroactive TB, so that the sensor had a low detection limit of 3.3×10^{-5} ng/mL. The results of recovery experiment exhibited excellent specificity and favorable spike recovery for ESAT-6 determination in real serum samples, which might provide a promising technology platform for timely and accurate identification of MTB

infection. We believe that with the discovery of new targets and nanomaterials, the sensitivity, specificity, detection limit, linear range, and other characteristic parameters of aptasensors will be significantly improved, and MTB detection methods with more clinical applicability will be developed.

Acknowledgements This work is supported by National Natural Science Foundation of China (81601856), the Third Batch of Young Backbone Teachers Funding Program in Colleges and Universities of Chongqing City ([2016] No. 53), Funds for Young Science and Technology Talent Cultivation Plan of Chongqing City (cstc2014kjrc-qnrc00004) and Fundamental and Advanced Research Projects of Chongqing City (cstc2016jcyjA0275).

Compliance with ethical standards The author(s) declare that they have no competing interests.

References

1. Zumla A, George A, Sharma V, Herbert R, BMo I, Oxley A, Oliver M (2015) The WHO 2014 global tuberculosis report–further to go. Lancet Glob Health 3(1):e10–e12
2. Golub JE, Bur S, Cronin WA, Gange S, Baruch N, Comstock GW, Chaisson RE (2006) Delayed tuberculosis diagnosis and tuberculosis transmission. Int J Tuberc Lung Dis 10(1):24–30
3. Elmasry S, Elkady I, Zaghloul MH, Albadrawey MK (2008) Rapid and simple detection of a mycobacterium circulating antigen in serum of pulmonary tuberculosis patients by using a monoclonal antibody and Fast-Dot-ELISA. Clin Biochem 41(3):145–151
4. Slogotskaya L, Bogorodskaya E, Sentchichina O, Nikitina G, Litvinov V, Seltsovsky P, Nikolenko N, Kudlay D (2016) Detection TB infection using a skin tests with tuberculin and allergen recombinant (CFP-10-ESAT-6) in children and adolescents in Moscow in 2015. Eur Respir J 48(suppl 60): OA3038
5. Wolf H, Mendez M, Gilman RH, Sheen P, Soto G, Velarde AK, Zimic M, Escombe AR, Montenegro S, Oberhelman RA (2008) Diagnosis of pediatric pulmonary tuberculosis by stool PCR. Am J Trop Med Hyg 79(6):893–898
6. Sarmiento OL, Weigle KA, Alexander J, Weber DJ, Miller WC (2003) Assessment by meta-analysis of PCR for diagnosis of smear-negative pulmonary tuberculosis. J Clin Microbiol 41(7): 3233–3240
7. Zhang SL, Zhao JW, Sun ZQ, Yang EZ, Yan JH, Qi Z, Zhang GL, Zhang HM, Qi YM, Wang HH (2009) Development and evaluation of a novel multiple-antigen ELISA for serodiagnosis of tuberculosis. Tuberculosis 89(4):278–284
8. Doherty TM, Demissie A, Menzies D, Andersen P, Rook G, Zumla A (2005) Effect of sample handling on analysis of cytokine responses to Mycobacterium tuberculosis in clinical samples using ELISA, ELISPOT and quantitative PCR. J Immunol Methods 298(1–2):129–141
9. Goletti D, Petruccioli E, Joosten SA, Ottenhoff THM (2016) Tuberculosis biomarkers: from diagnosis to protection. Infect Dis Rep 8(2):24–32
10. Tang XL, Zhou YX, Wu SM, Pan Q, Xia B, Zhang XL (2014) CFP10 and ESAT6 aptamers as effective mycobacterial antigen diagnostic reagents. J Infect 69(6):569–580
11. Pollock JM, Andersen P (1997) The potential of the ESAT-6 antigen secreted by virulent mycobacteria for specific diagnosis of tuberculosis. J Infect Dis 175(5):1251–1254
12. Hill PC, Jacksonsillah D, Fox A, Franken KL, Lugos MD, Jeffries DJ, Donkor SA, Hammond AS, Adegbola RA, Ottenhoff TH (2005) ESAT-6/CFP-10 fusion protein and peptides for optimal diagnosis of mycobacterium tuberculosis infection by ex vivo enzyme-linked immunospot assay in the Gambia. J Clin Microbiol 43(5):2070–2074
13. Guinn KM, Hickey MJ, Mathur SK, Zakel KL, Grotzke JE, Lewinsohn DM, Smith S, Sherman DR (2004) Individual RD1-region genes are required for export of ESAT-6/CFP-10 and for virulence of Mycobacterium tuberculosis. Mol Microbiol 51(2): 359–370
14. Diouani MF, Ouerghi O, Refai A, Belgacem K, Tlili C, Laouini D, Essafi M (2016) Detection of ESAT-6 by a label free miniature immuno-electrochemical biosensor as a diagnostic tool for tuberculosis. Mater Sci Eng C 74:465–470
15. Sepulveda D, Aroca MA, Varela A, Del PP, Osma JF (2017) Bioelectrochemical detection of Mycobacterium tuberculosis ESAT-6 in an antibody-based biomicrosystem. Sensors 17(10):2178
16. Cho EJ, Lee JW, Ellington AD (2009) Applications of Aptamers as sensors. Annu Rev Anal Chem 2(1):241–264
17. Famulok M, Mayer G (2011) Aptamer modules as sensors and detectors. Acc Chem Res 44(12):1349–1358
18. Bai L, Chai Y, Pu X, Yuan R (2014) A signal-on electrochemical aptasensor for ultrasensitive detection of endotoxin using three-way DNA junction-aided enzymatic recycling and graphene nanohybrid for amplification. Nanoscale 6(5):2902–2908
19. Wang G, Su X, Xu Q, Xu G, Lin J, Luo X (2017) Antifouling aptasensor for the detection of adenosine triphosphate in biological media based on mixed self-assembled aptamer and zwitterionic peptide. Biosens Bioelectron 101:129–134
20. Bai L, Yuan R, Chai Y, Zhuo Y, Yuan Y, Wang Y (2012) Simultaneous electrochemical detection of multiple analytes based on dual signal amplification of single-walled carbon nanotubes and multi-labeled graphene sheets. Biomaterials 33(4):1090–1096
21. Bai L, Chen Y, Bai Y, Chen Y, Zhou J, Huang A (2017) Fullerene-doped polyaniline as new redox nanoprobe and catalyst in electrochemical aptasensor for ultrasensitive detection of Mycobacterium tuberculosis MPT64 antigen in human serum. Biomaterials 133:11–19
22. Li WH, Ding K, Tian HR, Yao MS, Nath B, Deng WH, Wang Y, Xu G (2017) Conductive metal-organic framework nanowire array electrodes for high-performance solid-state supercapacitors. Adv Funct Mater 27(27):1702067
23. Sheberla D, Bachman JC, Elias JS, Sun CJ, Yang SH, Dincă M (2017) Conductive MOF electrodes for stable supercapacitors with high areal capacitance. Nat Mater 16(2):220–224
24. Ke F, Wang L, Zhu J (2015) Multifunctional Au-Fe3O4@MOF core-shell nanocomposite catalysts with controllable reactivity and magnetic recyclability. Nanoscale 7(3):1201–1208
25. Tang Z, He J, Chen J, Niu Y, Zhao Y, Zhang Y, Yu C (2018) A sensitive sandwich-type immunosensor for the detection of galectin-3 based on N-GNRs-Fe-MOFs@AuNPs nanocomposites and a novel AuPt-methylene blue nanorod. Biosens Bioelectron 101:253–259
26. Guo Y, Sun X, Liu Y, Wang W, Qiu H, Gao J (2012) One pot preparation of reduced graphene oxide (RGO) or Au (Ag) nanoparticle-RGO hybrids using chitosan as a reducing and stabilizing agent and their use in methanol electrooxidation. Carbon 50(7):2513–2523
27. Wang Y, Hu S (2006) A novel nitric oxide biosensor based on electropolymerization poly(toluidine blue) film electrode and its

application to nitric oxide released in liver homogenate. Biosens Bioelectron 22(1):10–17
28. Jia H, Chang G, Shu H, Xu M, Wang X, Zhang Z, Liu X, He H, Wang K, Zhu R (2017) Pt nanoparticles modified Au dendritic nanostructures: facile synthesis and enhanced electrocatalytic performance for methanol oxidation. Int J Hydrog Energy 42(34): 22100–22107
29. Ataeeesfahani H, Wang L, Nemoto Y, Yamauchi Y (2010) Synthesis of bimetallic Au@Pt nanoparticles with Au Core and nanostructured Pt Shell toward highly active Electrocatalysts. Chem Mater 22(23):6310–6318
30. Thakur H, Kaur N, Sabherwal P, Sareen D, Prabhakar N (2017) Aptamer based voltammetric biosensor for the detection of Mycobacterium tuberculosis antigen MPT64. Microchim Acta 184(7):1–8
31. Thakur H, Kaur N, Sareen D, Prabhakar N (2017) Electrochemical determination of M. tuberculosis antigen based on Poly(3,4-ethylenedioxythiophene) and functionalized carbon nanotubes hybrid platform. Talanta 171:115–123
32. Ma Z, Qin L, Wang Y (2007) Screening and affinity analysis of aptamers to ESAT-6 protein from Mycobacterium tuberculosis. Chin J Clin 1:45–48
33. Ma Z, He F, Qin L, Hu Z, Jiang Q (2011) Selection of aptamers to CFP10-ESAT6 protein from Mycobacterium tuberculosis. J Mol Diagn Ther 3(6):377–380
34. Chen J, Yu C, Zhao Y, Niu Y, Zhang L, Yu Y, Wu J, He J (2016) A novel non-invasive detection method for the FGFR3 gene mutation in maternal plasma for a fetal achondroplasia diagnosis based on signal amplification by hemin-MOFs/PtNPs. Biosens Bioelectron 91:892–899
35. Wang H, Hu Q, Meng Y, Jin Z, Fang Z, Fu Q, Gao W, Xu L, Song Y, Lu F (2018) Efficient detection of hazardous catechol and hydroquinone with MOF-rGO modified carbon paste electrode. J Hazard Mater 353:151–157